

System-Size Independence of Directed Flow Measured at the BNL Relativistic Heavy-Ion Collider

B. I. Abelev,¹⁰ M. M. Aggarwal,³² Z. Ahammed,⁴⁷ B. D. Anderson,²¹ D. Arkhipkin,¹⁴ G. S. Averichev,¹³ Y. Bai,³⁰ J. Balewski,²⁵ O. Barannikova,¹⁰ L. S. Barnby,² J. Baudot,¹⁹ S. Baumgart,⁵² D. R. Beavis,³ R. Bellwied,⁵⁰ F. Benedosso,³⁰ R. R. Betts,¹⁰ S. Bhardwaj,³⁷ A. Bhasin,²⁰ A. K. Bhati,³² H. Bichsel,⁴⁹ J. Bielcik,¹² J. Bielcikova,¹² B. Biritz,⁷ L. C. Bland,³ M. Bombara,² B. E. Bonner,³⁸ M. Botje,³⁰ J. Bouchet,²¹ E. Braidot,³⁰ A. V. Brandin,²⁸ S. Buehlmann,³ T. P. Burton,² M. Bystersky,¹² X. Z. Cai,⁴¹ H. Caines,⁵² M. Calderón de la Barca Sánchez,⁶ J. Callner,¹⁰ O. Catu,⁵² D. Cebra,⁶ R. Cendejas,⁷ M. C. Cervantes,⁴³ Z. Chajecki,³¹ P. Chaloupka,¹² S. Chattopadhyay,⁴⁷ H. F. Chen,⁴⁰ J. H. Chen,⁴¹ J. Y. Chen,⁵¹ J. Cheng,⁴⁵ M. Cherney,¹¹ A. Chikanian,⁵² K. E. Choi,³⁶ W. Christie,³ S. U. Chung,³ R. F. Clarke,⁴³ M. J. M. Codrington,⁴³ J. P. Coffin,¹⁹ T. M. Cormier,⁵⁰ M. R. Cosentino,³⁹ J. G. Cramer,⁴⁹ H. J. Crawford,⁵ D. Das,⁶ S. Dash,¹⁶ M. Daugherty,⁴⁴ M. M. de Moura,³⁹ T. G. Dedovich,¹³ M. DePhillips,³ A. A. Derevschikov,³⁴ R. Derradi de Souza,⁸ L. Didenko,³ T. Dietel,¹⁵ P. Djawotho,¹⁸ S. M. Dogra,²⁰ X. Dong,²⁴ J. L. Drachenberg,⁴³ J. E. Draper,⁶ F. Du,⁵² J. C. Dunlop,³ M. R. Dutta Mazumdar,⁴⁷ W. R. Edwards,²⁴ L. G. Efimov,¹³ E. Elhalhuli,² M. Elnimr,⁵⁰ V. Emelianov,²⁸ J. Engelage,⁵ G. Eppley,³⁸ B. Erazmus,⁴² M. Estienne,¹⁹ L. Eun,³³ P. Fachini,³ R. Fatemi,²² J. Fedorisin,¹³ A. Feng,⁵¹ P. Filip,¹⁴ E. Finch,⁵² V. Fine,³ Y. Fisyak,³ C. A. Gagliardi,⁴³ L. Gaillard,² D. R. Gangadharan,⁷ M. S. Ganti,⁴⁷ E. Garcia-Solis,¹⁰ V. Ghazikhanian,⁷ P. Ghosh,⁴⁷ Y. N. Gorbunov,¹¹ A. Gordon,³ O. Grebenyuk,³⁰ D. Grosnick,⁴⁶ B. Grube,³⁶ S. M. Guertin,⁷ K. S. F. F. Guimaraes,³⁹ A. Gupta,²⁰ N. Gupta,²⁰ W. Guryn,³ B. Haag,⁶ T. J. Hallman,³ A. Hamed,⁴³ J. W. Harris,⁵² W. He,¹⁸ M. Heinz,⁵² S. Heppelmann,³³ B. Hippolyte,¹⁹ A. Hirsch,³⁵ A. M. Hoffman,²⁵ G. W. Hoffmann,⁴⁴ D. J. Hofman,¹⁰ R. S. Hollis,¹⁰ H. Z. Huang,⁷ E. W. Hughes,⁴ T. J. Humanic,³¹ G. Igo,⁷ A. Iordanova,¹⁰ P. Jacobs,²⁴ W. W. Jacobs,¹⁸ P. Jakl,¹² F. Jin,⁴¹ P. G. Jones,² E. G. Judd,⁵ S. Kabana,⁴² K. Kajimoto,⁴⁴ K. Kang,⁴⁵ J. Kapitan,¹² M. Kaplan,⁹ D. Keane,²¹ A. Kechechyan,¹³ D. Kettler,⁴⁹ V. Yu. Khodyrev,³⁴ J. Kiryluk,²⁴ A. Kisiel,³¹ S. R. Klein,²⁴ A. G. Knospe,⁵² A. Kocoloski,²⁵ D. D. Koetke,⁴⁶ T. Kollegger,¹⁵ M. Kopytine,²¹ L. Kotchenda,²⁸ V. Kouchpil,¹² P. Kravtsov,²⁸ V. I. Kravtsov,³⁴ K. Krueger,¹ C. Kuhn,¹⁹ A. Kumar,³² L. Kumar,³² P. Kurnadi,⁷ M. A. C. Lamont,³ J. M. Landgraf,³ S. Lange,¹⁵ S. LaPointe,⁵⁰ F. Laue,³ J. Lauret,³ A. Lebedev,³ R. Lednicky,¹⁴ C-H. Lee,³⁶ M. J. LeVine,³ C. Li,⁴⁰ Y. Li,⁴⁵ G. Lin,⁵² X. Lin,⁵¹ S. J. Lindenbaum,²⁹ M. A. Lisa,³¹ F. Liu,⁵¹ J. Liu,³⁸ L. Liu,⁵¹ T. Ljubicic,³ W. J. Llope,³⁸ R. S. Longacre,³ W. A. Love,³ Y. Lu,⁴⁰ T. Ludlam,³ D. Lynn,³ G. L. Ma,⁴¹ J. G. Ma,⁷ Y. G. Ma,⁴¹ D. P. Mahapatra,¹⁶ R. Majka,⁵² L. K. Mangotra,²⁰ R. Manweiler,⁴⁶ S. Margetis,²¹ C. Markert,⁴⁴ H. S. Matis,²⁴ Yu. A. Matulenko,³⁴ T. S. McShane,¹¹ A. Meschanin,³⁴ J. Millane,²⁵ M. L. Miller,²⁵ N. G. Minaev,³⁴ S. Mioduszewski,⁴³ A. Mischke,³⁰ J. Mitchell,³⁸ B. Mohanty,⁴⁷ D. A. Morozov,³⁴ M. G. Munhoz,³⁹ B. K. Nandi,¹⁷ C. Nattrass,⁵² T. K. Nayak,⁴⁷ J. M. Nelson,² C. Nepali,²¹ P. K. Netrakanti,³⁵ M. J. Ng,⁵ L. V. Nogach,³⁴ S. B. Nurushev,³⁴ G. Odyniec,²⁴ A. Ogawa,³ H. Okada,³ V. Okorokov,²⁸ D. Olson,²⁴ M. Pachr,¹² S. K. Pal,⁴⁷ Y. Panebratsev,¹³ T. Pawlak,⁴⁸ T. Peitzmann,³⁰ V. Perevoztchikov,³ C. Perkins,⁵ W. Peryt,⁴⁸ S. C. Phatak,¹⁶ M. Planinic,⁵³ J. Pluta,⁴⁸ N. Poljak,⁵³ N. Porile,³⁵ A. M. Poskanzer,²⁴ M. Potekhin,³ B. V. K. S. Potukuchi,²⁰ D. Prindle,⁴⁹ C. Pruneau,⁵⁰ N. K. Pruthi,³² J. Putschke,⁵² I. A. Qattan,¹⁸ R. Raniwala,³⁷ S. Raniwala,³⁷ R. L. Ray,⁴⁴ A. Ridiger,²⁸ H. G. Ritter,²⁴ J. B. Roberts,³⁸ O. V. Rogachevskiy,¹³ J. L. Romero,⁶ A. Rose,²⁴ C. Roy,⁴² L. Ruan,³ M. J. Russcher,³⁰ V. Rykov,²¹ R. Sahoo,⁴² I. Sakrejda,²⁴ T. Sakuma,²⁵ S. Salur,²⁴ J. Sandweiss,⁵² M. Sarsour,⁴³ J. Schambach,⁴⁴ R. P. Scharenberg,³⁵ N. Schmitz,²⁶ J. Seger,¹¹ I. Selyuzhenkov,¹⁸ P. Seyboth,²⁶ A. Shabetai,¹⁹ E. Shahaliev,¹³ M. Shao,⁴⁰ M. Sharma,⁵⁰ S. S. Shi,⁵¹ X-H. Shi,⁴¹ E. P. Sichtermann,²⁴ F. Simon,²⁶ R. N. Singaraju,⁴⁷ M. J. Skoby,³⁵ N. Smirnov,⁵² R. Snellings,³⁰ P. Sorensen,³ J. Sowinski,¹⁸ H. M. Spinka,¹ B. Srivastava,³⁵ A. Stadnik,¹³ T. D. S. Stanislaus,⁴⁶ D. Staszak,⁷ R. Stock,¹⁵ M. Strikhanov,²⁸ B. Stringfellow,³⁵ A. A. P. Suaide,³⁹ M. C. Suarez,¹⁰ N. L. Subba,²¹ M. Sumbera,¹² X. M. Sun,²⁴ Y. Sun,⁴⁰ Z. Sun,²³ B. Surrow,²⁵ T. J. M. Symons,²⁴ A. Szanto de Toledo,³⁹ J. Takahashi,⁸ A. H. Tang,³ Z. Tang,⁴⁰ T. Tarnowsky,³⁵ D. Thein,⁴⁴ J. H. Thomas,²⁴ J. Tian,⁴¹ A. R. Timmins,² S. Timoshenko,²⁸ M. Tokarev,¹³ T. A. Trainor,⁴⁹ V. N. Tram,²⁴ A. L. Trattner,⁵ S. Trentalange,⁷ R. E. Tribble,⁴³ O. D. Tsai,⁷ J. Ulery,³⁵ T. Ullrich,³ D. G. Underwood,¹ G. Van Buren,³ N. van der Kolk,³⁰ M. van Leeuwen,³⁰ A. M. Vander Molen,²⁷ R. Varma,¹⁷ G. M. S. Vasconcelos,⁸ I. M. Vasilevski,¹⁴ A. N. Vasiliev,³⁴ F. Videbaek,³ S. E. Vigdor,¹⁸ Y. P. Viyogi,¹⁶ S. Vokal,¹³ S. A. Voloshin,⁵⁰ M. Wada,⁴⁴ W. T. Wagoner,¹¹ F. Wang,³⁵ G. Wang,⁷ J. S. Wang,²³ Q. Wang,³⁵ X. Wang,⁴⁵ X. L. Wang,⁴⁰ Y. Wang,⁴⁵ J. C. Webb,⁴⁶ G. D. Westfall,²⁷ C. Whitten, Jr.,⁷ H. Wieman,²⁴ S. W. Wissink,¹⁸ R. Witt,⁵² J. Wu,⁴⁰ Y. Wu,⁵¹ N. Xu,²⁴ Q. H. Xu,²⁴ Y. Xu,⁴⁰ Z. Xu,³ Y. Y. Yang,²³ P. Yepes,³⁸ I-K. Yoo,³⁶ Q. Yue,⁴⁵ M. Zawisza,⁴⁸ H. Zbroszczyk,⁴⁸ W. Zhan,²³ H. Zhang,³ S. Zhang,⁴¹ W. M. Zhang,²¹ Y. Zhang,⁴⁰ Z. P. Zhang,⁴⁰ Y. Zhao,⁴⁰ C. Zhong,⁴¹ J. Zhou,³⁸ R. Zoukarniev,¹⁴ Y. Zoukarnieva,¹⁴ and J. X. Zuo⁴¹

(STAR Collaboration)

- ¹Argonne National Laboratory, Argonne, Illinois 60439, USA
²University of Birmingham, Birmingham, United Kingdom
³Brookhaven National Laboratory, Upton, New York 11973, USA
⁴California Institute of Technology, Pasadena, California 91125, USA
⁵University of California, Berkeley, California 94720, USA
⁶University of California, Davis, California 95616, USA
⁷University of California, Los Angeles, California 90095, USA
⁸Universidade Estadual de Campinas, Sao Paulo, Brazil
⁹Carnegie Mellon University, Pittsburgh, Pennsylvania 15213, USA
¹⁰University of Illinois at Chicago, Chicago, Illinois 60607, USA
¹¹Creighton University, Omaha, Nebraska 68178, USA
¹²Nuclear Physics Institute AS CR, 250 68 Řež/Prague, Czech Republic
¹³Laboratory for High Energy (JINR), Dubna, Russia
¹⁴Particle Physics Laboratory (JINR), Dubna, Russia
¹⁵University of Frankfurt, Frankfurt, Germany
¹⁶Institute of Physics, Bhubaneswar 751005, India
¹⁷Indian Institute of Technology, Mumbai, India
¹⁸Indiana University, Bloomington, Indiana 47408, USA
¹⁹Institut de Recherches Subatomiques, Strasbourg, France
²⁰University of Jammu, Jammu 180001, India
²¹Kent State University, Kent, Ohio 44242, USA
²²University of Kentucky, Lexington, Kentucky, 40506-0055, USA
²³Institute of Modern Physics, Lanzhou, China
²⁴Lawrence Berkeley National Laboratory, Berkeley, California 94720, USA
²⁵Massachusetts Institute of Technology, Cambridge, Massachusetts 02139-4307, USA
²⁶Max-Planck-Institut für Physik, Munich, Germany
²⁷Michigan State University, East Lansing, Michigan 48824, USA
²⁸Moscow Engineering Physics Institute, Moscow Russia
²⁹City College of New York, New York City, New York 10031, USA
³⁰NIKHEF and Utrecht University, Amsterdam, The Netherlands
³¹Ohio State University, Columbus, Ohio 43210, USA
³²Panjab University, Chandigarh 160014, India
³³Pennsylvania State University, University Park, Pennsylvania 16802, USA
³⁴Institute of High Energy Physics, Protvino, Russia
³⁵Purdue University, West Lafayette, Indiana 47907, USA
³⁶Pusan National University, Pusan, Republic of Korea
³⁷University of Rajasthan, Jaipur 302004, India
³⁸Rice University, Houston, Texas 77251, USA
³⁹Universidade de Sao Paulo, Sao Paulo, Brazil
⁴⁰University of Science and Technology of China, Hefei 230026, China
⁴¹Shanghai Institute of Applied Physics, Shanghai 201800, China
⁴²SUBATECH, Nantes, France
⁴³Texas A&M University, College Station, Texas 77843, USA
⁴⁴University of Texas, Austin, Texas 78712, USA
⁴⁵Tsinghua University, Beijing 100084, China
⁴⁶Valparaiso University, Valparaiso, Indiana 46383, USA
⁴⁷Variable Energy Cyclotron Centre, Kolkata 700064, India
⁴⁸Warsaw University of Technology, Warsaw, Poland
⁴⁹University of Washington, Seattle, Washington 98195, USA
⁵⁰Wayne State University, Detroit, Michigan 48201, USA
⁵¹Institute of Particle Physics, CCNU (HZNU), Wuhan 430079, China
⁵²Yale University, New Haven, Connecticut 06520, USA
⁵³University of Zagreb, Zagreb, HR-10002, Croatia

(Received 10 July 2008; published 16 December 2008)

We measure directed flow (v_1) for charged particles in Au + Au and Cu + Cu collisions at $\sqrt{s_{NN}} = 200$ and 62.4 GeV, as a function of pseudorapidity (η), transverse momentum (p_T), and collision centrality, based on data from the STAR experiment. We find that the directed flow depends on the incident energy but, contrary to all available model implementations, not on the size of the colliding system at a given centrality. We extend the validity of the limiting fragmentation concept to v_1 in different collision systems, and investigate possible explanations for the observed sign change in $v_1(p_T)$.

The heavy-ion program at the Relativistic Heavy-Ion Collider (RHIC) seeks to understand the nature and dynamics of strongly interacting matter under extreme conditions. It is widely expected that in collisions at RHIC, a new partonic phase of matter is created, strongly interacting quark gluon plasma [1]. In particular, its bulk nature is revealed in strong *elliptic* flow, which in central collisions approaches the predictions of ideal hydrodynamics, assuming system thermalization on an extremely short time scale (~ 0.5 fm/c) [2]. However, the mechanism behind such rapid thermalization remains far from clear and is under active theoretical study [3–5]. This may be related to another novel phenomenon that could be relevant at RHIC—saturation of the gluon distribution—which characterizes the nuclear parton distribution prior to collision [6]. Various theoretical approaches to connect collision geometry, saturated gluon distributions, and the onset of bulk collective behavior are being explored [2]; more experimental input would guide these efforts.

Directed flow refers to collective sideways deflection of particles and is characterized by a *first-order* harmonic (v_1) of the Fourier expansion of particle's azimuthal distribution with respect to the reaction plane [7]. At large η (in the fragmentation region) the directed flow is believed to be generated during the nuclear passage time ($2R/\gamma \sim 0.1$ fm/c) [8,9]. It therefore probes the onset of bulk collective dynamics during thermalization, providing valuable experimental guidance to models of the preequilibrium stage. In this Letter, we present multiple-differential measurements of v_1 for Au + Au and Cu + Cu collisions at $\sqrt{s_{NN}} = 200$ and 62.4 GeV as a function of η , p_t , and collision centrality. Here, we report an intriguing new universal scaling of the phenomenon with collision centrality. Existing implementations of Boltzmann or cascade and hydrodynamic models are unable to explain the measured trends.

At RHIC energies, it is a challenge to measure v_1 accurately due to the relatively small signal and a potentially large systematic error arising from nonflow (azimuthal correlations not related to the reaction plane orientation). In this work, the reaction plane was determined from the sideward deflection of spectator neutrons [9,10] measured in the Shower Maximum Detectors (SMD) of the Zero Degree Calorimeters (ZDC) [11,12]. The v_1 based on this quantity, denoted $v_1\{\text{ZDC-SMD}\}$ [11], should have minimal contribution from nonflow effects due to the large η gap between the spectator neutrons used to establish the reaction plane and the η region where the measurements were performed.

Charged-particle tracks were reconstructed in STAR's main time projection chamber (TPC) [13] and forward TPCs [14], with pseudorapidity coverage $|\eta| < 1.3$ and $2.5 < |\eta| < 4.0$, respectively. The centrality definition (in

which zero represents the most central collisions) and track quality cuts are the same as in Ref. [15]. This study is based on Au + Au samples of 8×10^6 events at 200 GeV, 5×10^6 at 62.4 GeV, and Cu + Cu samples of 12×10^6 events at 200 GeV, and 8×10^6 at 62.4 GeV. All were obtained with a minimum-bias trigger. Systematic uncertainties on v_1 measurements are estimated to be within 10% for the η range studied. This limit is based on comparisons of $v_1\{\text{ZDC-SMD}\}$ and independent analysis methods [11,15], and we also make use of forward-backward symmetry to constrain estimates of systematic errors. Nonflow is not the dominant source of systematic uncertainty. More details about these errors can be found in Refs. [11,15].

The resolution [7] of the first-order event plane reconstructed using the ZDC-SMDs is a crucial quantity for this analysis. The magnitude of the event-plane resolution, defined as $\langle \cos(\Psi_{EP} - \Psi_{RP}) \rangle$ [7], increases with the spectator v_1 and the number of neutrons per event detected by the ZDC-SMDs. The ZDC size is optimized for 200 GeV, and its acceptance for spectator neutrons decreases at lower energies due to spectator neutrons being emitted within a cone whose apex angle increases with the inverse of the beam momentum. For the 30%–60% most central collisions, resolutions for 200 GeV Au + Au and Cu + Cu, and for 62.4 GeV Au + Au and Cu + Cu are about 0.4, 0.15, 0.15, and 0.04, respectively (more details are provided in Table 1 of Ref. [16]). The 30%–60% centrality interval is the only region where the ZDC-SMD event-plane resolution can be reliably determined for all four systems.

The charged particle $v_1(\eta)$ is shown in Fig. 1 for Au + Au at $\sqrt{s_{NN}} = 200$ GeV in three centralities. The inset

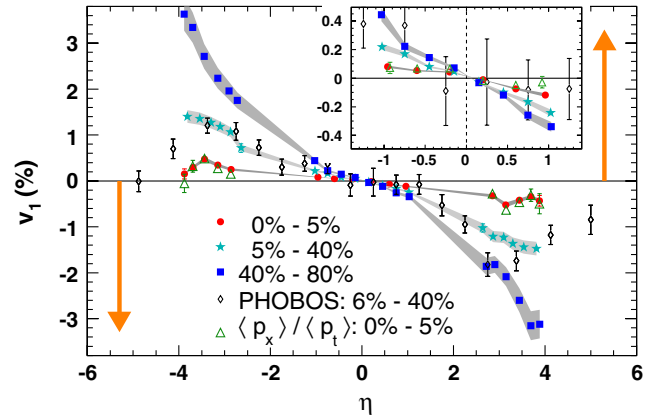


FIG. 1 (color online). Charged particle $v_1(\eta)$ for three centralities in Au + Au collisions at 200 GeV. The arrows indicate the algebraic sign of v_1 for spectator neutrons, and their positions on the η axis correspond to beam rapidity. The inset shows the mid- η region in more detail. The error bars are statistical, and the shaded bands show systematic errors. PHOBOS results [18] are also shown for midcentral collisions.

shows, on expanded scales, the mid- η region measured by the main TPC, where v_1 is resolvable below the 0.1% level. Within the studied η range, the sign of charged particle v_1 is opposite to that of the spectators, and the v_1 magnitude increases from central to peripheral collisions. For 0%–5% centrality, the slope $dv_1/d\eta$ changes sign above the middle of the forward time projection chamber (FTPC) pseudorapidity acceptance, and our results agree with the pattern reported by PHOBOS over a broader η range [17,18].

The ratio $\langle p_x \rangle / \langle p_t \rangle$ is shown in Fig. 1 for the most central data (0%–5%), in comparison to v_1 . Here, p_x refers to the in-plane component of a track’s transverse momentum, a quantity commonly used prior to the 1990s [10]. As elaborated below, there is interest in the behavior of both v_1 and $\langle p_x \rangle$ when $v_1(p_t)$ changes sign.

To further examine v_1 , the 200 GeV Au + Au data are divided into bins of p_t (Fig. 2). The upper and lower panels show results from the main TPC and the FTPCs, respectively. In the main TPC, $v_1(p_t)$ crosses zero at $1 < p_t < 2$ GeV/c for central and midcentral collisions. A zero-crossing behavior in $v_1(p_t)$ is necessarily exhibited by a hydrodynamic calculation in which $\langle p_x \rangle$, presumably imparted during the passing time of the initial-state nuclei, has been neglected and set equal to zero [19]. Because of the poor momentum resolution of the FTPCs at higher p_t , we cannot test the zero crossing at forward η . It is noteworthy that the observed $\langle p_x \rangle$, presented in Fig. 1, is far

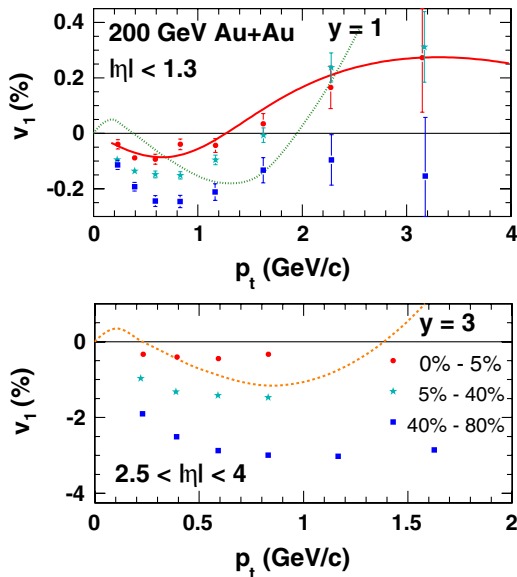


FIG. 2 (color online). Charged particle $v_1(p_t)$ in 200 GeV Au + Au for three centralities. The dashed curve and dotted curve are hydrodynamic calculations for the labeled rapidities at impact parameter 6.8 fm (15%–25% most central collisions). See the text for an explanation of the solid curve. The plotted error bars are statistical, and systematic errors (see Fig. 1) are within 10%.

from negligible, which contradicts the assumptions used in the hydrodynamic calculations.

The observed $v_1(p_t)$ dependence can be explained by assuming that pions and baryons flow with opposite sign, coupled with the measured baryon enhancement at higher p_t [20]. For example, taking linear functions [21] for pion and baryon $v_1(p_t)$, we obtain a satisfactory description of our data (see the solid curve in Fig. 2) with pion v_1 slopes, $dv_1/dp_t = -0.18 \pm 0.02$, -0.34 ± 0.02 , and -0.52 ± 0.04 , and baryon v_1 slopes 0.56 ± 0.12 , 0.86 ± 0.10 , and 1.02 ± 0.12 for centralities 0%–5%, 5%–40%, and 40%–80%, respectively. Note that the opposite v_1 slope for pions and protons, with the magnitude of proton slopes being larger, in this case is consistent with calculations [22] where the “wobble” rapidity dependence of identified particles has been predicted to result from the interplay of stopping and radial flow. Currently, we are unable to test the wobble effect in $v_1(\eta)$ with identified particles due to limited statistics and limited particle identification.

To study the energy and system-size dependence of v_1 , Fig. 3 shows Cu + Cu data compared to Au + Au in the centrality range 30%–60% for both 200 and 62.4 GeV. There is a clear trend for $v_1(\eta)$ to decrease with increasing beam energy for both Au + Au and Cu + Cu. In the studied pseudorapidity and centrality range, $v_1(\eta)$ is, within errors, independent of the system size at each beam energy, despite the three-to-one mass ratio between gold and copper. This remarkable feature holds for almost all centrality bins studied, as shown in Fig. 4, and persists even near mid- η (as shown in the upper panel), where elliptic flow (v_2) of charged particles in Cu + Cu is con-

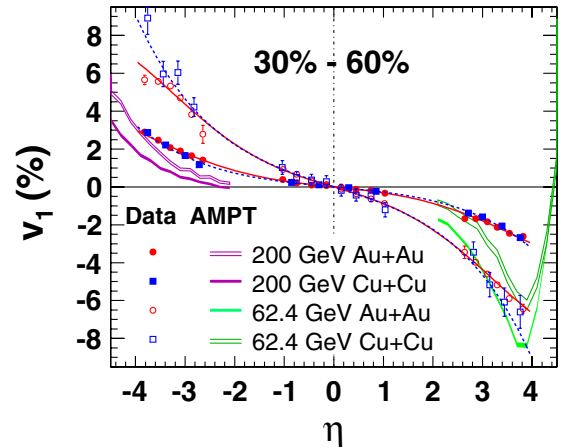


FIG. 3 (color online). Charged particle $v_1(\eta)$ for midcentral (30%–60%) Au + Au and Cu + Cu at 200 and 62.4 GeV. The solid curves and dashed curves are odd-order polynomial fits to guide the eye and demonstrate the forward-backward symmetry of the data. The wider shaded bands are from AMPT for the same conditions as the data. For clarity, 200 (62.4) GeV calculations are shown only at negative (positive) η . The plotted error bars are statistical, and systematic errors (see Figs. 1 and 5) are within 10%.

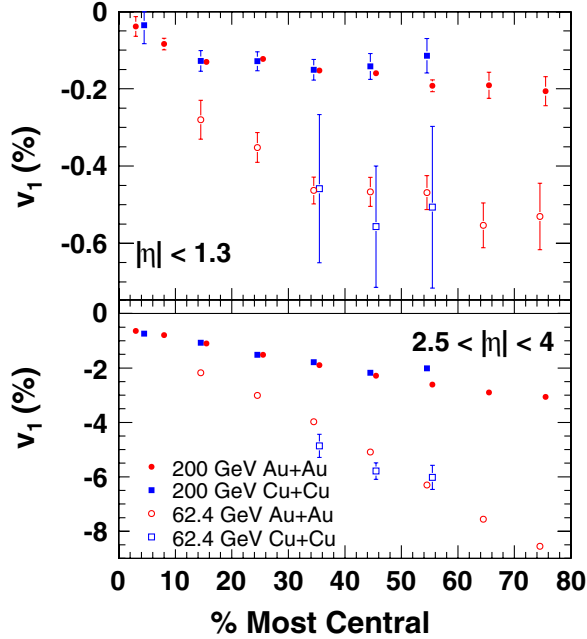


FIG. 4 (color online). Charged particle v_1 versus centrality, for Au + Au and Cu + Cu at 200 and 62.4 GeV. The upper (lower) panels show results from the main TPC (FTPC). The plotted error bars are statistical, and systematic errors (see Figs. 1 and 5) are within 10%.

siderably lower than in Au + Au [23]. Unlike v_2/ϵ , the ratio of the elliptic flow to the system initial eccentricity, which scales with the particle density in the transverse plane $(1/S)dN_{ch}/dy$ [24] (also interpreted to be the mid-rapidity area density [25] or the system length [26]), $v_1(\eta)$ at a given centrality is found to be independent of the system size, and varies only with the incident energy. The different scalings for v_2/ϵ and v_1 might arise from the way in which they are developed: to produce v_2 , many momentum exchanges among particles must occur (and the number of momentum exchanges is related to the participant density and the dimensions of the system), while to produce v_1 , an important feature of the collision process is that different rapidity losses need to occur (related to the incident energy) for particles at different distances from the center of the participant zone [22].

The hybrid transport model AMPT (a multiphase transport model) [27] lies consistently below the measured data, as evident from Fig. 3. STAR's prior v_1 study [11] in Au + Au at 62 GeV also showed this trend for AMPT and other transport models. It is noteworthy that AMPT does not exhibit the observed pattern of system-size independence. UrQMD (ultrarelativistic quantum molecular dynamics) [28] (not shown here) is similar to AMPT in exhibiting a significant change in v_1 between Au + Au and Cu + Cu.

Further scaling behavior is seen by transforming the data presented in Fig. 3 into the projectile frame (see Fig. 5), where zero on the horizontal axis corresponds to the beam rapidity, y_{beam} , for each of the collision energies. Within

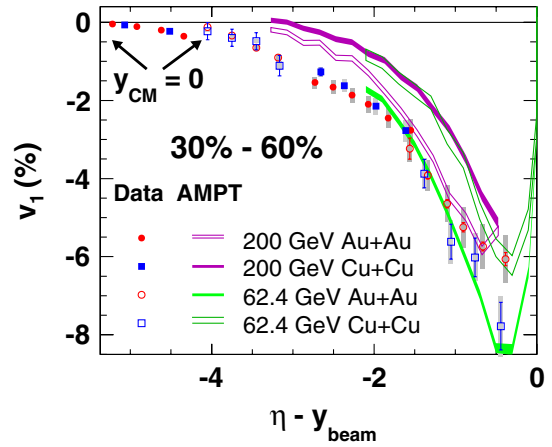


FIG. 5 (color online). Charged particle v_1 versus $\eta - y_{beam}$, for 30%–60% Au + Au and Cu + Cu at 200 and 62.4 GeV. The plotted error bars are statistical, and the shaded bars show systematic errors.

three units from y_{beam} , most data points lie on a universal curve for v_1 versus $\eta - y_{beam}$. This incident-energy scaling of directed flow has previously been reported for Au + Au [11,18], and it is now evident that the limiting fragmentation hypothesis [29] holds even for much lighter collision systems like Cu + Cu. AMPT adheres less closely to limiting fragmentation for Cu + Cu. Note that the quantity $\eta - y_{beam}$ introduces some uncertainty due to the use of η instead of rapidity; the latter requires particle identification. The system-size independence at a given fractional cross section and longitudinal scaling of scaled multiplicity distributions, $dN_{ch}/d\eta/(N_{part}/2)$, have been previously reported by the PHOBOS Collaboration [30].

In summary, we have presented measurements of charged-particle directed flow as a function of p_t , η , and centrality in Au + Au and Cu + Cu collisions at $\sqrt{s_{NN}} = 200$ and 62.4 GeV. The observed trend of decreasing v_1 with increasing beam energy agrees with models. The lack of system-size dependence in v_1 for Au + Au and Cu + Cu is quite remarkable and is a feature not observed or predicted by any existing model implementation. The presented η dependence of v_1 provides further support for limiting fragmentation scaling by extending its applicability to Cu + Cu. The observed p_t dependence of directed flow motivates further theoretical investigations and experimental measurements with identified particles.

We thank the RHIC Operations Group and RCF at BNL, and the NERSC Center at LBNL and the resources provided by the Open Science Grid consortium for their support. This work was supported in part by the Offices of NP and HEP within the U.S. DOE Office of Science, the U.S. NSF, the Sloan Foundation, the DFG Excellence Cluster EXC153 of Germany, CNRS/IN2P3, RA, RPL, and EMN of France, STFC and EPSRC of the United Kingdom, FAPESP of Brazil, the Russian Ministry of Science and

Technology, the NNSFC, CAS, MoST, and MoE of China, IRP and GA of the Czech Republic, FOM of the Netherlands, DAE, DST, and CSIR of the Government of India, Swiss NSF, the Polish State Committee for Scientific Research, Slovak Research and Development Agency, and the Korea Science and Engineering Foundation.

-
- [1] I. Arsene *et al.* (BRAHMS Collaboration), Nucl. Phys. **A757**, 1 (2005); B.B. Back *et al.* (PHOBOS Collaboration), Nucl. Phys. **A757**, 28 (2005); J. Adams *et al.* (STAR Collaboration), Nucl. Phys. **A757**, 102 (2005); K. Adcox *et al.* (PHENIX Collaboration), Nucl. Phys. **A757**, 184 (2005).
- [2] P. Kolb and U. Heinz, arXiv:nucl-th/0305084; P. Huovinen and P. V. Ruuskanen, Annu. Rev. Nucl. Part. Sci. **56**, 163 (2006).
- [3] Y. V. Kovchegov and A. Taliotis, Phys. Rev. C **76**, 014905 (2007).
- [4] S. Mrowczynski, Proc. Sci. CPOD2006 (2006) 042.
- [5] A. H. Mueller, Nucl. Phys. **A702**, 65 (2002).
- [6] L. D. McLerran and R. Venugopalan, Phys. Rev. D **50**, 2225 (1994).
- [7] A. M. Poskanzer and S. A. Voloshin, Phys. Rev. C **58**, 1671 (1998).
- [8] H. Sorge, Phys. Rev. Lett. **78**, 2309 (1997).
- [9] N. Herrmann, J. P. Wessels, and T. Wienold, Annu. Rev. Nucl. Part. Sci. **49**, 581 (1999).
- [10] W. Reisdorf and H. G. Ritter, Annu. Rev. Nucl. Part. Sci. **47**, 663 (1997).
- [11] J. Adams *et al.* (STAR Collaboration), Phys. Rev. C **73**, 034903 (2006).
- [12] C. Adler *et al.*, Nucl. Instrum. Methods Phys. Res., Sect. A **470**, 488 (2001); The STAR ZDC-SMD has the same structure as the STAR EEMC (end cap electromagnetic calorimeter) SMD: C. E. Allgower *et al.*, Nucl. Instrum. Methods Phys. Res., Sect. A **499**, 740 (2003); STAR ZDC-SMD proposal, STAR Note SN-0448, 2003.
- [13] M. Anderson *et al.*, Nucl. Instrum. Methods Phys. Res., Sect. A **499**, 659 (2003).
- [14] K. H. Ackermann *et al.*, Nucl. Instrum. Methods Phys. Res., Sect. A **499**, 713 (2003).
- [15] J. Adams *et al.* (STAR Collaboration), Phys. Rev. C **72**, 014904 (2005).
- [16] G. Wang, J. Phys. G **34**, S1093 (2007).
- [17] B. B. Back *et al.* (PHOBOS Collaboration), J. Phys. G **30**, S1243 (2004).
- [18] B. B. Back *et al.* (PHOBOS Collaboration), Phys. Rev. Lett. **97**, 012301 (2006).
- [19] U. Heinz and P. Kolb, J. Phys. G **30**, S1229 (2004).
- [20] J. Adams *et al.* (STAR Collaboration), Phys. Lett. B **655**, 104 (2007).
- [21] S. Voloshin *et al.* (E877 Collaboration), Nucl. Phys. **A638**, 455c (1998).
- [22] R. J. M. Snellings, H. Sorge, S. A. Voloshin, F. Q. Wang, and N. Xu, Phys. Rev. Lett. **84**, 2803 (2000).
- [23] B. Alver *et al.* (PHOBOS Collaboration), Phys. Rev. Lett. **98**, 242302 (2007); S. A. Voloshin, J. Phys. G **34**, S883 (2007).
- [24] S. A. Voloshin and A. M. Poskanzer, Phys. Lett. B **474**, 27 (2000).
- [25] C. Adler *et al.* (STAR Collaboration), Phys. Rev. C **66**, 034904 (2002); G. Roland (PHOBOS Collaboration), Nucl. Phys. **A774**, 113 (2006).
- [26] A. H. Tang, J. Phys. G **34**, S277 (2007).
- [27] Z. W. Lin and C. M. Ko, Phys. Rev. C **65**, 034904 (2002); L.-W. Chen and C.-M. Ko, J. Phys. G **31**, S49 (2005).
- [28] S. A. Bass *et al.*, Prog. Part. Nucl. Phys. **41**, 255 (1998); M. Bleicher *et al.*, J. Phys. G **25**, 1859 (1999).
- [29] J. Benecke, T. T. Chou, C.-N. Yang, and E. Yen, Phys. Rev. **188**, 2159 (1969).
- [30] B. Alver (PHOBOS Collaboration), arXiv:0709.4008.